ARTICLES
PUBLISHED ONLINE: 23 SEPTEMBER 2009 | DOI: 10.1038/NCHEM.366
nature chemistry

Geometric and electronic structure and reactivity of a mononuclear 'side-on' nickel(III)–peroxo complex

Jaeheung Cho[1], Ritimukta Sarangi[2], Jamespandi Annaraj[1], Sung Yeon Kim[1], Minoru Kubo[3], Takashi Ogura[3], Edward I. Solomon[2,4]* and Wonwoo Nam[1]*

Metal-dioxygen adducts, such as metal-superoxo and -peroxo species, are key intermediates often detected in the catalytic cycles of dioxygen activation by metalloenzymes and biomimetic compounds. The synthesis and spectroscopic characterization of an end-on nickel(II)-superoxo complex with a 14-membered macrocyclic ligand was reported previously. Here we report the isolation, spectroscopic characterization, and high-resolution crystal structure of a mononuclear side-on nickel(III)-peroxo complex with a 12-membered macrocyclic ligand, $[Ni(12\text{-}TMC)(O_2)]^+$ (1) (12-TMC = 1,4,7,10-tetramethyl-1,4,7,10-tetraazacyclododecane). In contrast to the end-on nickel(II)-superoxo complex, the nickel(III)-peroxo complex is not reactive in electrophilic reactions, but is capable of conducting nucleophilic reactions. The nickel(III)-peroxo complex transfers the bound dioxygen to manganese(II) complexes, thus affording the corresponding nickel(II) and manganese(III)-peroxo complexes. Our results demonstrate the significance of supporting ligands in tuning the geometric and electronic structures and reactivities of metal–O_2 intermediates that have been shown to have biological as well as synthetic usefulness in biomimetic reactions.

Metalloenzymes activate dioxygen (O_2) to carry out a variety of biological reactions including biotransformation of naturally occurring molecules, oxidative metabolism of xenobiotics, and oxidative phosphorylation. One goal in biomimetic research is to understand the mechanistic details of dioxygen activation and oxygenation reactions and the structures of reactive intermediates formed at the active sites of the metalloenzymes[1]. In the unified mechanism of dioxygen activation, dioxygen first binds to a reduced metal centre that forms metal-superoxo and -peroxo intermediates, after which oxygen-oxygen bond cleavage leads to the formation of high-valent metal-oxo species that are believed to carry out substrate oxidation[1]. Among the metal-oxygen intermediates, mononuclear metal-O_2 adducts, such as metal-superoxo and -peroxo species, have attracted much attention as key intermediates in the catalytic cycles of dioxygen activation by metalloenzymes, including haem and non-haem iron and copper enzymes[2–4].

In biomimetic and synthetic chemistry, mononuclear metal-O_2 complexes, including titanium, vanadium, chromium, manganese, iron, cobalt, nickel, copper and the second and third row transition metals, have been synthesized and characterized using various spectroscopic techniques and X-ray crystallography, and their reactivities have been extensively investigated in nucleophilic and electrophilic oxidation reactions[5–11]. A notable example is the mononuclear copper-O_2 species, which shows a diverse and rich chemistry in structures, spectroscopic properties and reactivities[10–16]. X-ray crystal structures of side-on (η^2) and end-on (η^1) copper(II)-superoxo and side-on (η^2) copper(III)-peroxo complexes were successfully obtained[17–19], and the mode of O_2 coordination (for example, side-on versus end-on O_2 binding) and the electronic nature of the copper–O_2 core (for example, copper(II)-superoxo versus copper(III)-peroxo) were found to vary depending on the supporting ligands of the copper complexes[20–23].

In the case of mononuclear nickel-O_2 intermediates, side-on and end-on nickel(II)-superoxo and side-on nickel(II)-peroxo complexes have been characterized by spectroscopic, X-ray crystallographic, and computational methods[24–27]. The nickel(II)-superoxo complexes showed electrophilic reactivity, such as the oxidation of PPh_3 to $OPPh_3$[24–26]. However, to the best of our knowledge, the crystal structure and reactivity of a mononuclear nickel(III)-peroxo complex have not yet been reported. In this study, we have examined the effects of supporting ligands on the mode of O_2 coordination and the electronic structure of the nickel-O_2 moiety in mononuclear nickel-O_2 complexes, by varying the ring size of the macrocyclic ligand coordinated in $[Ni(II)(14\text{-}TMC)(O_2)]^+$ (**2**) (14-TMC = 1,4,8,11-tetramethyl-1,4,8,11-tetraazacyclotetradecane), which was characterized as an end-on nickel(II)-superoxo complex by spectroscopic and computational methods[25]. We now report for the first time the synthesis, spectroscopic and electronic properties, and crystal structure of a mononuclear side-on (η^2) nickel(III)-peroxo complex stabilized by a 12-membered macrocyclic ligand, $[Ni(III)(12\text{-}TMC)(O_2)]^+$ (**1**) (12-TMC = 1,4,7,10-tetramethyl-1,4,7,10-tetraazacyclododecane). The reactivities of the nickel(III)-peroxo complex in electrophilic and nucleophilic reactions and peroxo group transfer to other metal complexes have been discussed.

Results and discussion

The starting nickel complex, $[Ni(12\text{-}TMC)(CH_3CN)]^{2+}$ (**3**), was synthesized and characterized with UV–vis absorption spectroscopy, electrospray ionization mass spectrometry (ESI-MS), and X-ray crystallography (see Supplementary Information, Figs S1 and S2, Tables S1 and S2). The reaction of **3** with five equivalents of H_2O_2 in the presence of two equivalents of triethylamine (Et_3N) in CH_3CN at 0 °C produces a green intermediate, **1**, which exhibits distinct absorption features that are different from those of **2** (Fig. 1)[25]. The intermediate persisted for several days at 25 °C, and the greater

[1]Department of Chemistry and Nano Science, Department of Bioinspired Science, Center for Biomimetic Systems, Ewha Womans University, Seoul 120-750, Korea, [2]Stanford Synchrotron Radiation Lightsource, SLAC National Accelerator Laboratory, Menlo Park, California 94025, USA, [3]Picobiology Institute, Graduate School of Life Science, University of Hyogo, Hyogo 678-1297, Japan, [4]Department of Chemistry, Stanford University, Stanford, California 94305, USA. *e-mail: wwnam@ewha.ac.kr; edward.solomon@stanford.edu

© 2009 Macmillan Publishers Limited. All rights reserved.

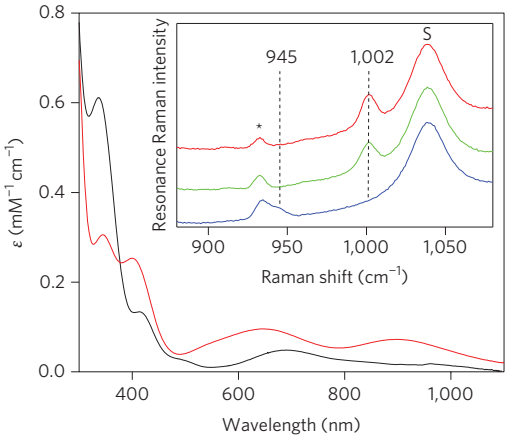

Figure 1 | Characterization of 1. Electronic absorption spectra of **1** (red solid line) and **2** (black solid line) in CH_3CN at 0 °C. Inset shows resonance Raman spectra of **1** (32 mM) obtained upon excitation at 442 nm in CD_3CN at −20 °C; isolated **1** (red line) and *in situ*-generated **1** prepared with $H_2{}^{16}O_2$ (green line) and $H_2{}^{18}O_2$ (blue line). The peak marked with 'S' is ascribed to d_3-acetonitrile solvent and an asterisk denotes a band derived from a nickel complex bearing a 12-TMC ligand. ε, molar absorption coefficient.

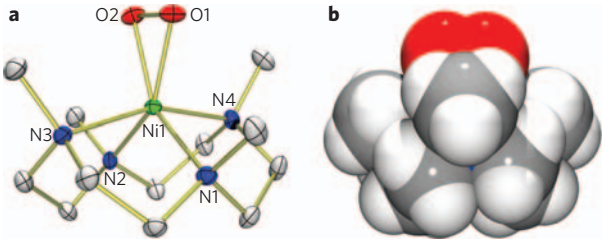

Figure 2 | X-ray crystal structure of 1. a, ORTEP plot of $[Ni(12\text{-}TMC)(O_2)]^+$ (**1**) with thermal ellipsoids drawn at the 30% probability level. Hydrogen atoms are omitted for clarity. **b**, Side view (space-filling representation) of **1**, derived from the crystal structure determination. Selected bond lengths (Å) and angles (°): Ni–O1 1.884(3), Ni–O2 1.894(3), Ni–N1 2.027(3), Ni–N2 2.038(3), Ni–N3 2.160(3), Ni–N4 2.158(3), O1–O2 1.386(4); O1–Ni–O2 43.04(11), Ni–O1–O2 68.87(16), Ni–O2–O1 68.09(15). The crystallographic data have been deposited with the Cambridge Crystallographic Data Centre under CCDC 719999.

thermal stability of **1** allowed us to isolate crystals, which were used in spectroscopic and structural analyses and reactivity studies. The ESI-MS of **1** exhibits a prominent ion peak at a mass-to-charge (m/z) ratio of 318.0 (see Supplementary Fig. S3a), whose mass and isotope distribution pattern correspond to $[Ni(12\text{-}TMC)(O_2)]^+$ (calculated m/z of 318.2) (see Supplementary Fig. S3a, inset). When the reaction was carried out with isotopically labelled $H_2{}^{18}O_2$, a mass peak corresponding to $[Ni(12\text{-}TMC)(^{18}O_2)]^+$ appeared at a m/z of 322.0 (calculated m/z of 322.2) (see Supplementary Fig. S3a, inset). The shift in four mass units on substitution of ^{16}O with ^{18}O indicates that **1** contains an O_2 unit. The electron paramagnetic resonance spectrum of a frozen acetonitrile solution of **1** measured at 4.3 K exhibits a rhombic signal with g values of 2.22, 2.17 and 2.06 (see Supplementary Fig. S3b), which is indicative of a $(d_z^2)^1$ electron configuration typically observed for nickel(III) species[28], nickel(II)-superoxo complexes[24–26] and a six-coordinated bis(μ-superoxo)Ni_2(II) complex[29]. The room temperature magnetic moment of 2.13 μ_B, determined using the ^1H NMR Evans method[30], is consistent with an $S = 1/2$ ground state for **1**.

The resonance Raman spectrum of **1** was collected using 442-nm excitation at −20 °C. **1** prepared with $H_2{}^{16}O_2$ exhibits an isotopically sensitive band at 1,002 cm^{-1}, which shifts to 945 cm^{-1} when $H_2{}^{18}O_2$ is used, consistent with its assignment as an O–O stretching vibration on the basis of its $^{16}\Delta - {}^{18}\Delta$ value of 57 cm^{-1} ($^{16}\Delta - {}^{18}\Delta$ (calculated) = 57 cm^{-1}) (Fig. 1, inset). Interestingly, the observed O–O stretching frequency of **1**(1,002 cm^{-1}) is significantly lower than that of **2** (1,131 cm^{-1})[25], but is between the superoxo (that is, ν_{OO} of ∼1,050–1,200 cm^{-1}) and peroxo (that is, ν_{OO} of ∼800–930 cm^{-1}) categories[31]. It is also worth noting that the O–O stretching frequency of **1** is quite close to those observed in copper(III)-peroxo species (∼970 cm^{-1})[18,22]. Thus, the resonance Raman spectroscopic data suggests that the O_2 in **1** has significant peroxo character, $O_2{}^{2-}$.

The X-ray crystal structure of **1**-(ClO_4)·CH_3CN revealed the mononuclear side-on 1:1 nickel complex of O_2 in a distorted octahedral geometry arising from the triangular NiO_2 moiety with a small bite angle of 43.04(11)° (Fig. 2). Notably, the O–O bond length (1.386(4) Å) of **1** is longer than those of Ni(II)-superoxo complexes, such as **2** (1.301 Å, from density functional theory (DFT) calculations)[25] and Ni(II)(O_2) with a β-diketiminato ligand (1.347 Å)[26]; the O–O bond length of **1** is between those of metal-superoxo compounds (∼1.2–1.3 Å) and metal-peroxo compounds (∼1.4–1.5 Å)[31], but closer to the metal-peroxo category. For comparison, an O–O bond length of 1.392 Å was reported in a Cu(III)-peroxo complex[22]. In addition, the Ni–O average bond of **1** (1.889 Å) is shorter than that of **2** (1.984 Å, from DFT calculations)[25], supporting a nickel(III) formulation. In conjunction with the low O–O stretching frequency measured by Raman spectroscopy, the structural data, such as O–O and Ni–O bond distances, suggest that **1** can be formulated as a nickel(III)-peroxo species, Ni(III)-$(O_2{}^{2-})$.

Ni K-edge X-ray absorption spectroscopy was then performed to directly probe the oxidation state of nickel and the ligand field of the nickel centre. The normalized Ni K-edge X-ray absorption spectra of **1** and **2** are presented in Fig. 3. The inset shows the expanded pre-edge region. The pre-edge features are due to an electric dipole-forbidden quadrupole-allowed $1s \rightarrow 3d$ transition[32]. The energy position of the pre-edge transition is dominantly affected by changes in ligand field at the absorbing nickel centre and increases with an increase in ligand field[23]. The pre-edge transitions in **1** and **2** occur at 8332.3 eV and 8331.6 eV, respectively, indicating an increase in ligand field on going from **2** to **1** (Fig. 3). The Ni K-edge energy position increases with an increase in Q_{Ni}, the charge on the absorbing nickel centre in the complex. Typically,

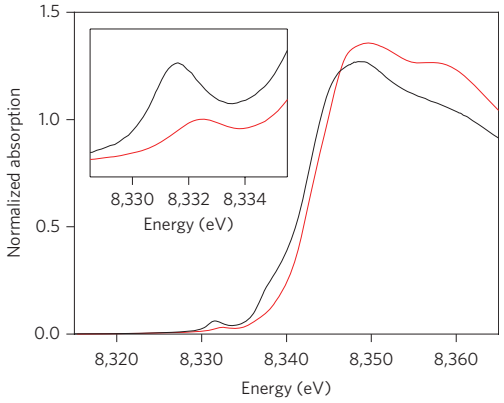

Figure 3 | Ni K-edge X-ray absorption spectra of 1 (red) and 2 (black). The inset shows the expanded pre-edge region. The Ni K-edge X-ray absorption spectrum of **2** was reported previously in ref. 18. Owing to large differences in the beamline optics, cryostat temperatures, and detection methods, the data were re-measured in the present study for accurate comparison of **1** and **2** under identical conditions.

© 2009 Macmillan Publishers Limited. All rights reserved.

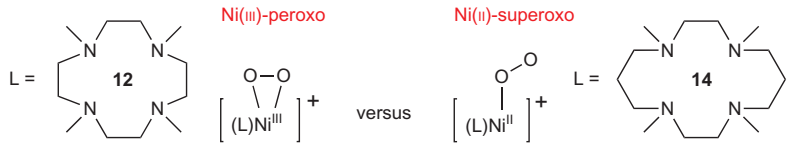

Figure 4 | Formation of Ni(III)-peroxo versus Ni(II)-superoxo intermediates. The geometric and electronic structures of nickel-O_2 intermediates are determined by the ring-size of the macrocyclic ligands, such as a Ni(III)-peroxo complex with a 12-membered macrocyclic ligand and a Ni(II)-superoxo complex with a 14-membered macrocyclic ligand.

for nickel complexes, the K-edge first-maxima do not show a large change with Q_{Ni} (ref. 33); however, as seen in Fig. 3 the first-maximum is shifted ~1.8 eV from **2** to **1**, clearly indicating an increase in Q_{Ni} in **1** compared with **2**. Ni K-edge extended X-ray absorption fine structure (EXAFS) data and their analyses show that the first shell coordination has increased from five in **2** to six in **1** (see Supplementary Figs. S4–S6, Tables S3 and S4), yet the Ni–O bond distance is ~0.06 Å shorter in **1** than in **2**. Together, the Ni K-edge and EXAFS data support a unique Ni(III)-(O_2^{2-}) description for **1**. These data, combined with the crystal structure, indicate that the O_2 binds side-on to the nickel centre in **1**, whereas the O_2 is end-on bound in **2** as previously reported[25]. This binding mode difference is accompanied by an electronic structure change from Ni(II)-(O_2^{-}) in **2** to Ni(III)-(O_2^{2-}) in **1**.

Density functional theory calculations were performed to understand the role of the macrocyclic ring in determining the geometric and electronic structures of **1** and **2** (see Supplementary Fig. S7 and Table S5 for structural details). The geometry-optimized structures of **1** and **2** show that the smaller 12-membered ring in **1** leads to contraction of the trans Ni–N bond angles. This displaces the nickel out of the N_1–N_2–N_3–N_4 plane and allows for its facile side-on overlap with the O_2. The side-on coordination of the O_2 in **1** allows for a stronger overlap of its π^* orbital with the nickel $3d_{x^2-y^2}$ orbital. This stronger σ overlap leads to the relative destabilization of the nickel $3d_{x^2-y^2}$ orbital, which results in the transfer of charge from the nickel $3d_{x^2-y^2}$ orbital to the O_2 to give a stable Ni(III)-(O_2^{2-}) species. We therefore conclude, based on the spectroscopic results, X-ray crystallography and DFT calculations, that **1** is best described as a mononuclear nickel(III)-peroxo complex. The role of the supporting ligand, 12-TMC, is to sterically allow O_2 to bind in a side-on fashion, resulting in more sigma antibonding interaction with the $3d_{x^2-y^2}$ orbital as indicated above. It also stabilizes the high oxidation state of Ni^{3+}, owing to the stronger interaction of the $Ni–N_{equatorial}$ bond (2.06 Å) in **1** compared with the $Ni–N_{equatorial}$ bond (2.14 Å from DFT calculations) in **2** (see Supplementary Table S5). Thus, as discussed in the mononuclear copper-O_2 chemistry[10–17,20,23], the geometric and electronic structures of nickel-O_2 species are modulated by the nature of supporting ligands (Fig. 4).

The reactivity of **2** was investigated in electrophilic and nucleophilic reactions. First, the electrophilic character of **1** was tested in the oxidation of PPh_3, thioanisole and xanthene. On addition of the substrates to a solution of **2** in CH_3CN at 25 °C, the intermediate remained intact without showing any absorption spectral changes, and product analysis of the reaction solutions revealed that no oxygenated products were formed in the reactions. These results demonstrate that **2** is not capable of conducting electrophilic oxidation under the reaction conditions. In contrast, nickel(II)-superoxo complexes have shown reactivities in electrophilic reactions, such as the oxidation of PPh_3[25,26] and xanthene (W.N. *et al.*, unpublished observations).

The nucleophilic character of **1** was investigated in aldehyde deformylation, with precedents that metal(III)-peroxo complexes with haem and non-haem ligands react with aldehydes to give the corresponding deformylated products[6,34,35]. On addition of 2-phenylpropionaldehyde (2-PPA) to **1** in CH_3CN at 25 °C, the characteristic UV–vis absorption bands of **1** disappeared with a first-order decay profile (see Supplementary Fig. S8a), and pseudo-first-order rate constants increased proportionally with the aldehyde concentration ($k_2 = 4.0 \times 10^{-2}\,M^{-1}\,s^{-1}$ at 25 °C) (see Supplementary Fig. S8b). Similar results were obtained in the reactions of cyclohexanecarboxaldehyde (CCA) but with a faster rate ($k_2 = 2.0 \times 10^{-1}\,M^{-1}\,s^{-1}$ at −10 °C) (see Supplementary Fig. S9). Product analysis of the resulting solutions revealed the formation of acetophenone (92% based on **1**) and cyclohexene (85% based on **1**) in the reactions of 2-PPA and CCA, respectively. The reactivity of **1** was further investigated using substituted benzaldehydes with a series of electron-donating and -withdrawing substituents at the *para* position of the phenyl group (*para*-Y-Ph-CHO; Y = Me, F, H, Br, Cl) (see Supplementary Fig. S10). A positive ρ^+ value of 6.1 in the Hammett plot was obtained, which is consistent with the nucleophilic character of the nickel(III)-O_2 unit involved in the oxidation of aldehydes.

More interestingly, we have observed a complete intermolecular O_2 transfer from **1** to different transition metal complexes, such as $[Mn(II)(14\text{-TMC})]^{2+}$ (**4**) (Fig. 5). Addition of **4** to a solution of **1** afforded changes in the absorption spectrum that are consistent with transfer of the O_2 from **1** to **4**, thereby producing **3** and a manganese(III)-peroxo complex, $[Mn(III)(14\text{-TMC})(O_2)]^{+}$ (**5**) (Fig. 6)[35]. Well-defined isosbestic points were observed at 416 and 687 nm in the titration reaction (Fig. 6). The intermolecular O_2 transfer from **1** to **4** was further confirmed by ESI-MS of the reaction

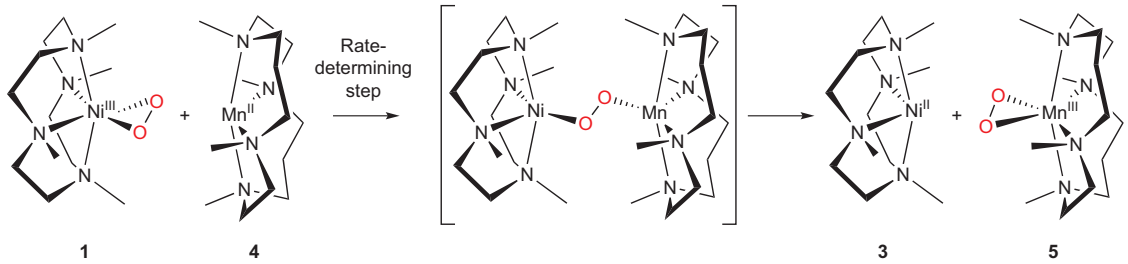

Figure 5 | Reaction scheme showing an intermolecular O_2 transfer between metal complexes. An O_2 group is transferred from $[Ni(III)(12\text{-TMC})(O_2)]^{+}$ (**1**) to $[Mn(II)(14\text{-TMC})]^{2+}$ (**4**) via a $[(12\text{-TMC})Ni\text{-}O_2\text{-}Mn(14\text{-TMC})]^{3+}$ transition state, and the final products are $[Ni(II)(12\text{-TMC})]^{2+}$ (**3**) and $[Mn(III)(14\text{-TMC})(O_2)]^{+}$ (**5**).

© 2009 Macmillan Publishers Limited. All rights reserved.

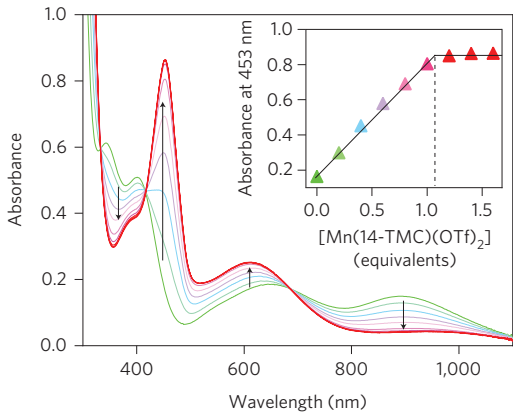

Figure 6 | Spectral evidence for an intermolecular O_2 transfer from 1 to 4. UV–vis spectral changes showing the formation of $[Mn(14\text{-}TMC)(O_2)]^+$ (**5**) (red) and the disappearance of $[Ni(III)(12\text{-}TMC)(O_2)]^+$ (**1**) (green) by addition of $[Mn(II)(14\text{-}TMC)]^{2+}$ (**4**) to a solution of **1** in increments of 0.2 equivalents in CH_3CN at 25 °C. Inset shows the spectroscopic titration at 453 nm for the formation of **5** as a function of the equivalents of **4** added to a solution of **1** in increments of 0.2.

solution, in which the mass peak corresponding to **1** disappeared with a concomitant appearance of mass peaks corresponding to **3** and **5** (see Supplementary Fig. S11). When the O_2 transfer reaction was carried out under an $^{18}O_2$ atmosphere, the product **5** did not contain the isotopically labelled $^{18}O_2$ group, demonstrating that molecular oxygen was not involved in the peroxo transfer reaction. As the peroxo transfer reaction was fast at 25 °C in CH_3CN, kinetic studies were performed in acetone at −50 °C. Upon addition of ten equivalents of **4** to the solution of **1**, **1** disappeared with a first-order decay profile (see Supplementary Fig. S12a).

Pseudo-first-order fitting of the kinetic data allowed us to determine the k_{obs} value to be $1.7(2) \times 10^{-3}$ s^{-1} at −50 °C (see Supplementary Fig. S12a, inset). The first-order rate constants increased proportionally with the concentration of **4**, giving a second-order rate constant of 2.0×10^{-1} M^{-1} s^{-1} at −50 °C (see Supplementary Fig. S12b). The rates were dependent on reaction temperatures, from which a linear Eyring plot was obtained between −60 and −30 °C to give the activation parameters of $\Delta H^{\ddagger} = 49$ kJ mol^{-1} and $\Delta S^{\ddagger} = -76$ J mol^{-1} K^{-1} (see Supplementary Fig. S12c). The observed second order kinetics and significant negative entropy value indicate that a bimolecular mechanism is operating in the O_2 transfer reaction, where the formation of the $[(12\text{-}TMC)Ni\text{-}O_2\text{-}Mn(14\text{-}TMC)]^{3+}$ intermediate is presumed to be the rate-determining step (Fig. 5).

Finally, we found that the reverse reaction, which is the peroxo transfer from **5** to **3**, does not occur. In this section, we have shown the first example of the complete O_2 transfer between metal complexes. The observation of the complete O_2 transfer from a nickel(III)-peroxo complex to a manganese(II) complex is different from the behaviour of other systems; in the reactions of mononuclear $M\text{-}O_2$ adducts (M = Cu and Ni) and a second metal complex, M or M′, formation of homo- or hetero-dinuclear complexes comprising $[M_2(\mu\text{-}O)_2]^{n+}$, $[M_2(O_2)]^{n+}$ or $[MM'(\mu\text{-}O)_2]^{n+}$ cores is observed[18,24,36,37]. The formation of $(Porp)Fe(III)\text{-}(O_2^{2-})\text{-}Cu(II)(L)$ complexes has also been observed in the reactions of iron(III)-peroxo porphyrins with copper(II)(L) complexes as chemical models of cytochrome *c* oxidase[38]. Detailed mechanistic investigations are underway in this laboratory to elucidate the difference between the complete O_2 transfer and the O_2-bridged dinuclear formation occurring in the reactions of mononuclear metal–O_2 and second metal complexes.

In conclusion, a mononuclear side-on nickel(III)-peroxo complex was successfully synthesized by varying the supporting ligand of the previously reported nickel(II)-superoxo complex (that is, the ring-size of the macrocyclic ligand). Combined with the precedents of mononuclear copper–O_2 intermediates[14,17,18], the present results highlight the importance of supporting ligands in determining geometric and electronic structures of mononuclear nickel-O_2 complexes (that is, nickel(III)-peroxo versus nickel(II)-superoxo species). Whether other factors, such as solvents, influence the geometric and electronic structures of nickel–O_2 complexes will be the subject of future studies.

The reactivities of nickel(III)-peroxo and nickel(II)-superoxo complexes were compared in electrophilic and nucleophilic reactions. In contrast to nickel(II)-superoxo complexes, which show reactivities in oxidative electrophilic reactions[24], the nickel(III)-peroxo complex is not reactive in electrophilic reactions but is capable of deformylating aldehydes through nucleophilic reactions. The observation of complete O_2 transfer between metal complexes is unprecedented; whether this is a general feature in other metal–O_2 adducts requires further experimental and computational study.

Methods

See experimental section in Supplementary Information for detailed experimental conditions and procedures, spectroscopic and kinetics analyses, and computational calculations.

Received 10 March 2009; accepted 12 August 2009; published online 23 September 2009

References

1. Nam, W. (ed.) Special issue on dioxygen activation by metalloenzymes and models. *Acc. Chem. Res.* **40,** 465–634 (2007).
2. Unno, M., Chen, H., Kusama, S., Shaik, S. & Ikeda-Saito, M. Structural characterization of the fleeting ferric peroxo species in myoglobin: experiment and theory. *J. Am. Chem. Soc.* **129,** 13394–13395 (2007).
3. Kovaleva, E. G. & Lipscomb, J. D. Crystal structures of Fe^{2+} dioxygenase superoxo, alkylperoxo, and bound product intermediates. *Science* **316,** 453–457 (2007).
4. Prigge, S. T., Eipper, B. A., Mains, R. E. & Amzel, L. M. Dioxgyen binds end-on to mononuclear copper in a precatalytic enzyme complex. *Science* **304,** 864–867 (2004).
5. Klotz, I. M. & Kurtz, D. M. Jr (eds) Special issue on metal-dioxygen complexes. *Chem. Rev.* **94,** 567–856 (1994).
6. Wertz, D. L. & Valentine, J. S. Nucleophilicity of iron-peroxo porphyrin complexes. *Struct. Bonding* **97,** 37–60 (2000).
7. Girerd, J.-J., Banse, F. & Simaan, A. J. Characterization and properties of non-heme iron peroxo complexes. *Struct. Bonding* **97,** 145–177 (2000).
8. Bakac, A. Kinetic and mechanistic studies of the reactions of transition metal-activated oxygen with inorganic substrates. *Coord. Chem. Rev.* **250,** 2046–2058 (2006).
9. Hikichi, S., Akita, M. & Moro-oka, Y. New aspects of the cobalt-dioxygen complex chemistry opened by hydrotris(pyrazoly)borate ligands (Tp^R): unique properties of Tp^RCo-dioxygen complexes. *Coord. Chem. Rev.* **198,** 61–87 (2000).
10. Mirica, L. M., Ottenwaelder, X. & Stack, T. D. P. Structure and spectroscopy of copper−dioxygen complexes. *Chem. Rev.* **104,** 1013–1045 (2004).
11. Lewis E. A. & Tolman, W. B. Reactivity of dioxygen-copper systems. *Chem. Rev.* **104,** 1047–1076 (2004).
12. Hatcher, L. Q. & Karlin, K. D. Oxidant types in copper-dioxygen chemistry: the ligand coordination defines the $Cu_n\text{-}O_2$ structure and subsequent reactivity. *J. Biol. Inorg. Chem.* **9,** 669–683 (2004).
13. Itoh, S. Mononuclear copper active-oxygen complexes. *Curr. Opin. Chem. Biol.* **10,** 115–122 (2006).
14. Cramer, C. J. & Tolman, W. B. Mononuclear $Cu-O_2$ complexes: geometries, spectroscopic properties, electronic structures, and reactivity. *Acc. Chem. Res.* **40,** 601–608 (2007).
15. Rolff, M. & Tuczek, F. How do copper enzymes hydroxylate aliphatic substrates? Recent insights from the chemistry of model systems. *Angew. Chem. Int. Ed.* **47,** 2344–2347 (2008).
16. Chen, P. & Solomon, E. I. O_2 activation by binuclear Cu sites: noncoupled versus exchange coupled reaction mechanisms. *Proc. Natl Acad. Sci. USA* **101,** 13105–13110 (2004).
17. Fujisawa, K., Tanaka, M., Moro-oka, Y. & Kitajima, N. A monomeric side-on superoxocopper(II) complex: $Cu(O_2)(HB(3\text{-}tBu\text{-}5\text{-}iPrpz)_3)$. *J. Am. Chem. Soc.* **116,** 12079–12080 (1994).
18. Spencer, D. J. E., Aboelella, N. W., Reynolds, A. M., Holland, P. L. & Tolman, W. B. β-Diketiminate ligand backbone structural effects on $Cu(I)/O_2$ reactivity: unique copper−superoxo and bis(μ-oxo) complexes. *J. Am. Chem. Soc.* **124,** 2108–2109 (2002).

© 2009 Macmillan Publishers Limited. All rights reserved.

19. Würtele, C. *et al.* Crystallographic characterization of a synthetic 1:1 end-on copper dioxygen adduct complex. *Angew. Chem. Int. Ed.* **45,** 3867–3869 (2006).
20. Gherman, B. F. & Cramer, C. J. Modeling the peroxide/superoxide continuum in 1:1 side-on adducts of O_2 with Cu. *Inorg. Chem.* **43,** 7281–7283 (2004).
21. Aboelella, N. W. *et al.* Dioxygen activation at a single copper site: structure, bonding, and mechanism of formation of 1:1 Cu-O_2 Adducts. *J. Am. Chem. Soc.* **126,** 16896–16911 (2004).
22. Reynolds, A. M., Gherman, B. F., Cramer, C. J. & Tolman, W. B. Characterization of a 1:1 Cu-O_2 adduct supported by an anilido imine ligand. *Inorg. Chem.* **44,** 6989–6997 (2005).
23. Sarangi, R. *et al.* X-ray absorption edge spectroscopy and computational studies on $LCuO_2$ species: superoxide − Cu^{II} versus peroxide − Cu^{III} bonding. *J. Am. Chem. Soc.* **128,** 8286–8296 (2006).
24. Kieber-Emmons, M. T. & Riordan, C. G. Dioxygen activation at monovalent nickel. *Acc. Chem. Res.* **40,** 618–625 (2007).
25. Kieber-Emmons, M. T. *et al.* Identification of an "end-on" nickel−superoxo adduct, $[Ni(TMC)(O_2)]^+$. *J. Am. Chem. Soc.* **128,** 14230–14231 (2006).
26. Yao, S., Bill, E., Milsmann, C., Wieghardt, K. & Driess, M. A 'side-on' superoxonickel complex $[LNi(O_2)]$ with a square-planar tetracoordinate nickel(II) center and its conversion into $[LNi(\mu\text{-}OH)_2NiL]$. *Angew. Chem. Int. Ed.* **47,** 7110–7113 (2008).
27. Matsumoto, M. & Nakatsu, K. Dioxygen-bis-(t-butylisocyanide)nickel. *Acta Cryst.* **B31,** 2711–2713 (1975).
28. Haines, R. I. & McAuley, A. Synthesis and reactions of nickel(III) complexes. *Coord. Chem. Rev.* **39,** 77–119 (1981).
29. Cho, J. *et al.* Sequential reaction intermediates in aliphatic C − H bond fuctionalization initiated by a bis(μ-oxo)dinickel(III) complex. *Inorg. Chem.* **45,** 2873–2885 (2006).
30. Evans, D. F. & Jakubovic, D. A. Water-soluble hexadentate Schiff-base lignads as sequestrating agents for iron(III) and gallium(III). *J. Chem. Soc. Dalton Trans.* 2927–2933 (1988).
31. Cramer, C. J., Tolman, W. B., Theopold, K. H. & Rheingold, A. L. Varible character of O−O and M−O bonding in side-on (η^2) 1:1 metal complexes of O_2. *Proc. Natl Acad. Sci. USA* **100,** 3635–3640 (2003).
32. Shulman, R. G., Yafet, Y., Eisenberger, P. & Blumberg, W. E. Observation and interpretation of X-ray absorption edges in iron compounds and proteins. *Proc. Natl Acad. Sci. USA* **73,** 1384–1388 (1976).
33. Colpas, G. J. *et al.* X-ray spectroscopic studies of nickel complexes, with application to the structure of nickel sites in hydrogenases. *Inorg. Chem.* **30,** 920–928 (1991).
34. Vaz, A. D. N., Roberts, E. S. & Coon, M. J. Olefin formation in the oxidative deformylation of aldehydes by cytochrome P-450. Mechanistic implications for catalysis by oxygen-derived peroxide. *J. Am. Chem. Soc.* **113,** 5886–5887 (1991).
35. Seo, M. S. *et al.* $[Mn(TMC)(O_2)]^+$: a side-on peroxido manganese(III) complex bearing a non-heme ligand. *Angew. Chem. Int. Ed.* **46,** 377–380 (2007).
36. Kieber-Emmons, M. T., Schenker, R., Yap, G. P. A., Brunold, T. C. & Riordan, C. G. Spectroscopic elucidation of a peroxo $Ni_2(\mu\text{-}O_2)$ intermediate derived from a nickel(I) complex and dioxygen. *Angew. Chem. Int. Ed.* **43,** 6716–6718 (2004).
37. Aboelella, N. W. *et al.* Mixed metal bis(μ-oxo) complexes with $[CuM(\mu\text{-}O)_2]^{n+}$ (M = Ni(III) or Pd(II)) cores. *Chem. Commun.* 1716–1717 (2004).
38. Chufán, E. E., Puiu, S. C. & Karlin, K. D. Heme − copper/dioxygen adduct formation, properties, and reactivity. *Acc. Chem. Res.* **40,** 563–572 (2007).

Acknowledgements

The research was supported by KOSEF/MEST of Korea through the CRI and WCU (R31-2008-000-10010-0) Programs (W.N.), SBS Foundation (W.N.), the Ministry of Education, Culture, Sports, Science and Technology of Japan through the Global COE program and Priority Area (No. 20050029) (T.O.), and NIH grant DK-31450 (E.I.S.). SSRL operations are funded by the Department of Energy, Office of Basic Energy Sciences. The SSRL Structural Molecular Biology program is supported by the National Institutes of Health, National Center for Research Resources, Biomedical Technology Program, and the Department of Energy, Office of Biological and Environmental Research.

Author contributions

J.C., E.I.S., and W.N. conceived and designed the experiments; J.C., R.S., J.A., S.Y.K., and M.K. performed the experiments; J.C., R.S., J.A., M.K., and T.O. analysed the data; J.C., R.S., E.I.S., and W.N. co-wrote the paper.

Additional information

Supplementary information and chemical compound information accompany this paper at www.nature.com/naturechemistry. Reprints and permission information is available online at http://npg.nature.com/reprintsandpermissions/. Correspondence and requests for materials should be addressed to E.I.S. and W.N.

© 2009 Macmillan Publishers Limited. All rights reserved.